A Comparative Study of Imidazolium-Based Ionic Liquid-Single-Walled Carbon Nanotube Composites with Enhanced Conductivity Properties for Supercapacitor Applications

Tirandai Hemraj-Benny[a], Sharon I. Lall-Ramnarine[a], Sophia N. Suarez[b], Domenec Paterno[b], Jasodra D. Ramdihal[a], Rawlric Sumner[a], Katelyn Urena[a], and James F. Wishart[c]

[a]Department of Chemistry, Queensborough Community College of the City University of New York, Bayside, New York 11364, USA
[b]Department of Physics, Brooklyn College of the City University of New York, Brooklyn, New York 11210, USA
[c]Chemistry Division, Brookhaven National Laboratory, Upton, New York 11973, USA

Mixtures of ionic liquids (ILs) containing single-walled carbon nanotubes (SWCNTs) were prepared and characterized to obtain electrolytes with optimized transport properties for the use in energy storage devices such as supercapacitors. Imidazolium ILs bearing cations with side chains of different functionality, coupled with bis(trifluoromethylsulfonyl)amide (NTf_2^-) or bis(fluorosulfonyl)amide (FSA^-) anions, were used in mixtures containing up to 5 wt% SWCNTs. At and above 2 wt% nanotube loading, the mixtures exhibited higher conductivities than the pure ILs, in spite of the extremely high viscosities. Loadings of 5 wt% produced very high conductivities, and studies of the temperature dependence indicated a change in the charge transport mechanism between 2 and 5 wt% loading. At 5 wt% loading, the highest conductivities (up to 540 mS/cm at 25 °C) were obtained for the ILs containing the NTf_2^- anion. These results can significantly contribute to the development of improved energy storage devices.

Introduction

Due to growing global environmental concerns, there are increasing demands for environmentally-friendly, efficient, renewable energy storage devices (1-3). Batteries, fuel cells, and supercapacitors are useful energy storage devices that function on the principle of electrochemical energy conversion (1). Supercapacitors have many improved properties over batteries and fuel cells, which include higher power density, shorter charge time, and longer life cycles, and thus they have various potential applications (1-5). Supercapacitors can be used as power supplies in small portable devices, and they can be used to provide energy in rural areas where costly electrical infrastructures are not available. Moreover, supercapacitors have great potential in electric and hybrid vehicles due to their high power density, which is required for short-term acceleration and recovery of energy during braking (1). Still, the main hindrance to more extensive usage of supercapacitors is their modest energy densities (~0.005 to ~10 W h/kg) (2, 6), which are accomplished through either their electric double layers or Faradaic reaction charge storage mechanisms. The energy density E is determined by the specific capacitance C and the maximum working voltage V through the relationship: $E = ½ CV^2$. Generally, C

is related to the electrode and electrolyte properties, while V depends on those of the electrolyte. Therefore, the choice of electrode-electrolyte combination is extremely important in the performance and potential applications of the resulting supercapacitor.

For optimal operation, supercapacitors require electrodes with high surface area, high conductivity, and suitable temperature and chemical stability (1, 3, 7). Carbon-based nanomaterials have been considered as promising electrodes for supercapacitors due to their unique high surface area, high conductivity and stability properties and low cost (1, 4, 8, 9). Nevertheless, activated carbon and reduced graphene oxide electrodes have shown weak performance, respectively due to their irregular pore structure and lack of restacking ability during chemical processes, which prevents the availability of maximum surface area to the electrolyte ions, thereby limiting charge storage (1, 4, 10).

Carbon nanotubes can serve as more efficient electrodes in supercapacitors (10). A single-walled carbon nanotube (SWCNT) consists of a single graphene sheet seamlessly wrapped into a cylindrical tube (0.4 nm to 3 nm in diameter with lengths up to micrometers) which can be either metallic or semiconducting depending on its diameter and chirality (11). SWCNTs of various diameters are found in bundles held together by strong van der Waals forces in a 'spaghetti' network (10, 12). It is expected that electrical transport in such materials is dominated by the contained metallic nanotubes (13). In fact, the electrical conductivity of SWCNTs has been reported to range between 10^2 to 10^6 S/cm (14). Multi-walled carbon nanotubes (MWCNTs) are made of concentric cylinders placed around a common central core with outer diameters ranging from 5 to 100 nm and lengths of tens of microns (15, 16). In general, carbon nanotube electrodes in electrochemical devices have lower equivalent series resistance than activated carbon, and they have substantial capacitance (~15 to ~200 F/g) because electrolyte ions can easily penetrate the mesoporous network of the nanotubes where small separations of about one nanometer exist between the charge on carbon nanotube electrodes and the countercharge in the electrolytes (4, 8, 9, 15, 17). SWCNTs are considered to be superior to MWCNTs for energy storage applications due to their higher surface area (smaller diameter), and improved purity, structural integrity, and capacitance (180 and 102 F/g for SWCNT and MWCNT electrodes, respectively) (12, 15, 17, 18).

Optimized electrolytes for supercapacitors should have a wide potential window, high ionic conductivity, excellent electrochemical stability, small solvated ion radius, low equivalent series resistance, and low volatility and viscosity (19). Common supercapacitor electrolytes include aqueous solutions, organic solutions, and ionic liquids. Whereas the main limitation for aqueous electrolytes such as KOH and H_2SO_4 is their small potential window due to water decomposition (~ 1.2 V), the limitation for organic solvents such as acetonitrile lies in their high vapor pressure and flammability (2, 20, 21). Ionic liquids are optimal electrolytes for supercapacitors because of their low volatility, excellent thermal stability, and wide working voltage windows (22). However, they suffer from relatively low ionic conductivities, which directly affects their high power output and energy density.

The combination of ILs with SWCNTs presents researchers with materials having the attributes of the individual components as well as the expanded range of applications due to their tunable softness and electroconducting and thermoconducting properties (23, 24). While there have been numerous molecular dynamics simulations studies on these

systems (25), there is a lack of experimental data in the literature. Although there are variations in the results, a common theme that has emerged is the local IL/SWCNT environment having a higher-density, layered ion arrangement at the interface (26). Generally, when a liquid is confined to a solid surface, the resulting molecular arrangement differs from the bulk due to the combination of the restrictions in mobility of the ions at the solid interface, and the Coulombic interactions that exist between them and the counterions of the neighboring liquid interface. Inside the SWCNT, these result in 'solid-like' or 'solvation layers' that can extend for several molecular diameters from the interface (27, 28). This ordering of the liquid into 'solvation layers' is characterized by an oscillatory molecular density profile and is a common feature for many liquids, including polymer melts and molecular liquids (27). As you move away from the interface, the packing density decreases (29). This was the case for hexylmethylimidazolium bis(trifluoromethylsulfonyl)amide (Hmim NTf_2) IL inside a (20,20) CNT (29), and ethylmethylimidazolium tetrafluoroborate (Emim BF_4) inside (*n*,*n*) SWCNTs (30). In addition to this is the bulk IL environment, which numerous studies have shown depends on the combination of anion and cation (31, 32). It should be noted that there are two interfaces – inside and outside the SWCNT and that the behavior of the IL at the interfaces can differ depending on its characteristics, as well as those of the SWCNT.

ILs with imidazolium cations ($Rmim^+$) exhibit attractive properties for energy storage applications such as relatively lower viscosities and higher conductivities than most ammonium and pyrrolidinium ILs, and electrochemical windows greater than 4 V (20, 21). Moreover, imidazolium ILs are excellent solvents for the dispersion of SWCNT bundles. Imidazolium ILs have a strong affinity towards the π-electronic SWCNT surfaces, thus disrupting π-π stacking interactions among SWCNTs and enabling the unraveling of the nanotube bundles (24, 33, 34). However, there are few studies that specifically investigate the relationship between increased ionic conductivity of imidazolium ILs upon the incorporation of single-walled carbon nanotubes, which leads to improved energy densities in supercapacitors. Recently, Kong et al. observed that the addition of SWCNTs to Emim BF_4 (electrochemical window 4.2 V) directly improved the ionic conductivity of the IL, and consequently increased the capacitance, energy density and cycling stability of a supercapacitor (35). Specifically, 0.5 wt% SWCNTs were dispersed in Emim BF_4 by a sonication method, and a 38 % increase in ionic conductivity of the pure IL to 26 mS cm^{-1} was observed. The IL-SWCNT mixture exhibited a higher energy density (35 Wh/kg) than the pure Emim BF_4 IL (30 Wh/kg) at a power density of 30 W/kg. While this reported 17% performance increase upon adding SWCNTs to an IL is modest, we undertook the present study in the belief that better results could be obtained at higher SWCNT loadings, and that the role of imidazolium cation functional groups in mediating IL-SWCNT interactions should be studied in order to optimize mixture performance.

In this work, we investigate the effect of cation and anion types, and SWCNT concentration, on the ion transport properties of the IL-SWCNT mixtures. It is well known that the ionic conductivities of pure ILs can be altered by varying the side chains on the imidazolium cation ring (36-38). In addition, various IL anions have different de-bundling effects on single-walled carbon nanotubes, which may alter the conductivity properties of SWCNT-IL mixtures differently (34). In addition to the limited fundamental experimental data available on IL-SWCNT mixtures, there is also a knowledge gap concerning the influence of varying the side chains of the imidazolium cation on the

conductivity properties of IL-SWCNT composites. Therefore, for the first-time temperature-dependent electrochemical impedance spectroscopy (EIS) measurements were performed to understand the electron transfer properties of composites containing varying concentrations of SWCNTs in combination with ILs composed of $Rmim^+$ cations bearing side chains with different functionalities, (R = butyl (B), allyl (A), and 2-methoxyethyl (EOM)), coupled with NTf_2^- or bis(fluorosulfonyl)amide (FSA^-) anions (Figure 1).

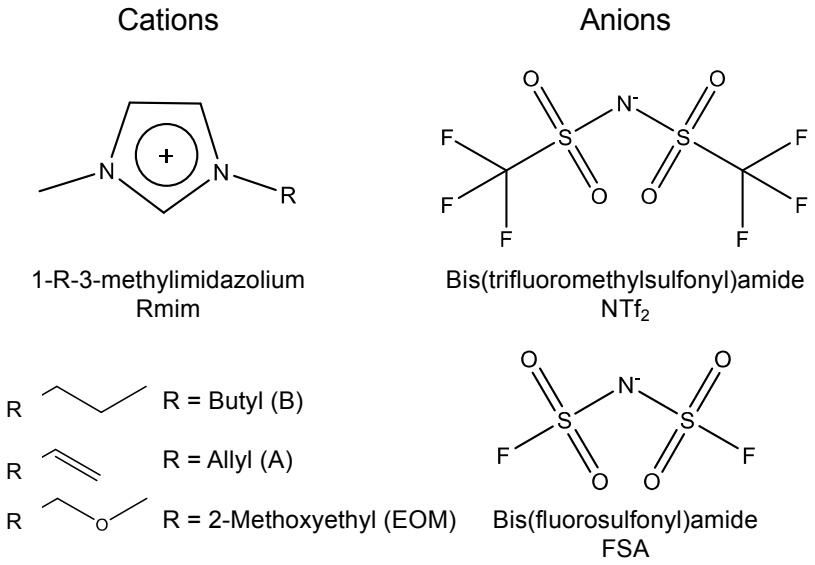

Figure 1. Structures of the ions used in this study.

The three functionalities were selected to vary the interionic interactions within the IL and the interactions between the IL cation and the SWCNT. $Bmim^+$ cation represents a standard 1-alkyl-3-methylimidazolium cation for baseline comparison, with an alkyl chain length short enough that the bulk IL is not divided into separate polar and non-polar domains (31) for better comparison to the other cations. $Amim^+$ cation includes a second unsaturated moiety in addition to the imidazolium cation head, to provide additional means of π-π interactions between the cation and the SWCNT. Ether-functionalized ILs containing cations such as $EOMmim^+$ are structured differently than their alkyl congeners because the ether group competes with the NTf_2^- or FSA^- anion for hydrogen bonding at the ring proton positions, with both intra- and intermolecular H-bonding modes (39-43). This difference in structure for the $EOMmim^+$ ILs may affect the way in which the cations interact with the SWCNT.

This study is one part of a series aimed at deciphering the IL-SWCNT interactions that govern the ion dynamics in these mixtures. Here we will focus almost exclusively on the ionic conductivity data, but our future publications will include temperature-dependent viscosity measurements as well as spectroscopic (Mid-IR and Raman) analyses.

Experimental

Materials. SWCNTs (CoMoCAT) (with a purity of > 95%, averaged diameter of 0.78 nm, median tube length of 1.5 μm, and specific surface area of 790 m^2/g) were obtained from Sigma Aldrich and were used without further purification. All chemicals used for the ionic liquid syntheses were of reagent grade, obtained from Sigma-Aldrich and used as received. ^1H and ^{13}C NMR spectra were recorded on a Bruker 400 MHz NMR spectrometer. Water contents of the synthesized pure ionic liquid samples were ≤ 70 ppm, as determined using a Mettler Toledo DL39 Karl Fischer Coulometer.

Ionic Liquid Synthesis

1a. Synthesis of 1-butyl-3-methylimidazolium bromide (Bmim Br)
1-methylimidazole (19.87 g, 0.2419 mol) dissolved in 50 mL acetonitrile was reacted with 10% excess of 2-bromoethylmethylether (34.80 g, 0.0.2540 mol) dissolved in 50 mL acetonitrile in a round bottom flask containing a stir bar and having a reflux condenser attached to it. The reaction was initiated at room temperature and left to stir for 3 days at 60 °C. The resulting halide salt was rotary evaporated and washed with ethyl acetate. The final product was a pale-yellow liquid (50.33 g, 95 %, molar mass: 219.12 g/mol). ^1H (400 MHz; D_2O) δ 0.94-0.98 (t, 3H), 1.32-1.41 (m, 2H), 1.86-1.93 (m, 2H), 3.94 (s, 3H), 4.23-4.27 (t, 2H), 7.48 (s, 1H), 7.54 (s, 1H), 8.77 (s, 1H); ^{13}C (101 MHz; D_2O) δ 12.71, 18.79, 31.30. 33.28, 49.32, 122.20, 123.45, 135.84.

2a. Synthesis of 1-(2-methoxyethyl)-3-methylimidazolium bromide (EOMmim Br)
1-methylimidazole (10.00 g, 0.1218 mol) dissolved in 25 mL acetonitrile was reacted with 10% excess of 2-bromoethylmethylether (18.62 g, 0.1218 mol) dissolved in 25 mL acetonitrile in a round bottom flask containing a stir bar and having a reflux condenser attached to it. The reaction was initiated at room temperature and left to stir for 5 days at 40 °C. The resulting halide salt was rotary evaporated and washed with ethyl acetate. The final product was a pale-yellow liquid (24.52 g, 92 %, molar mass: 221.10 g/mol). ^1H (400 MHz; D_2O) δ 3.40 (s, 3H), 3.84-3.87 (t, 2H), 3.92 (s, 3H), 4.40-4.42 (t, 2H), 7.47 (s, 1H), 7.52 (s, 1H); ^{13}C (101 MHz; D_2O) δ 0.84, 35.64, 48.83, 58.16, 69.76, 122.40, 123.45.

Preparation of Bis(trifluoromethylsulfonyl)amide Ionic Liquids

1b. Synthesis of 1-butyl-3-methylimidazolium bis(trifluoromethylsulfonyl)amide (Bmim NTf_2):1-butyl-3-methylimidazolium bromide (40.11 g, 0.1830 mol) dissolved in 90 mL deionized water was reacted with one equivalent of lithium bis(trifluoromethylsulfonyl)amide (52.56 g, 0.1830 mol) dissolved in 60 mL deionized water in a round bottom flask containing a stir bar. The reaction mixture was left to stir at room temperature for 24 hours. The resulting ionic liquid was washed with deionized water until the wash tested negative for residual bromide with 50 mM aqueous silver nitrate. The product was rotary evaporated and dried in a high vacuum oven at 60 ˚C for several days. The final product was a pale yellow, viscous liquid (71.94 g, 94 %, molar mass: 419.475 g/mol, water content: 23 ppm). ^1H (400 MHz; DMSO-d_6) δ 0.89-0.93 (t, 3H), 1.24-1.30 (m, 2H), 1.74-1.81 (m, 2H), 3.85 (s, 3H), 4.15-4.18 (t, 2H), 7.48 (s, 1H), 7.54 (s, 1H), 8.77 (s, 1H); ^{13}C (101 MHz; DMSO-d_6) δ 13.10, 18.70, 31.30, 35.63, 48.47, 114.64, 117.84, 121.04, 122.18, 123.54, 124.34, 136.45.

2b. Synthesis of 1-(2-methoxyethyl)-3-methylimidazolium bis(trifluoromethylsulfonyl) amide (EOMmim NTf_2)

1-(2-methoxyethyl)-3-methylimidazolium bromide (16.71 g, 0.07558 mol) dissolved in 20 mL deionized water was reacted with one equivalent of lithium bis(trifluoromethylsulfonyl)amide (21.71 g, 0.07558 mol) dissolved in 25 mL deionized water in a round bottom flask containing a stir bar. The reaction mixture was left to stir at room temperature for 24 hours. The resulting yellow ionic liquid was washed with deionized water until the wash tested negative for bromide with 50 mM aqueous silver nitrate. The product was rotary evaporated and dried in a high vacuum oven at 60 °C for several days. The final product was a pale-yellow viscous liquid (26.93 g, 85 %, molar mass: 421.33 g/mol, water content: 26 ppm). ^{1}H (400 MHz; DMSO-d_6) δ 3.08 (s, 3H), 3.67-3.70 (t, 2H), 3.88 (s, 3H), 4.37-4.39 (t, 2H), 7.49 (d, 1H), 8.00 (d, 1H), 9.24 (s, 1H), ^{13}C (101 MHz; DMSO-d_6) δ 36.2, 49.1,58.5, 60.2, 70.1, 114.6, 117.8, 121.0, 123.1, 123.9, 124.2, 137.3.

3b. Synthesis of 1-allyl-3-methylimidazolium bis(trifluoromethylsulfonyl)amide (Amim NTf_2)

1-allyl-3-methylimidazolium chloride (25.00 g, 0.1576 mol) dissolved in 30 mL deionized water was reacted with one equivalent of lithium bis(trifluoromethylsulfonyl)imide (45.26 g, 0.1576 mol) dissolved in 50 mL deionized water in a round bottom flask containing a stir bar. The reaction mixture was left to stir at room temperature for 24 hours. The resulting ionic liquid was washed with deionized water until the wash tested negative for residual chloride using 50 mM aqueous silver nitrate. The product was rotary evaporated and dried in a high vacuum oven at 70 ˚C for 48 hours. The final product was a very pale yellow, viscous liquid (59.79 g, 94%, molar mass: 403.31 g/mol, water content: 10 ppm). ^{1}H (400 MHz; DMSO-d_6) δ 3.85 (t,3H), 4.83-4.84 (d, 2H), 5.28-5.38 (m, 2H), 5.99-6.09 (1H, m), 7.69 (1H, s), 7.70 (1H, s), 9.09 (1H, s), ^{13}C (101 MHz; DMSO-d_6) δ 35.77, 50.81, 114.70, 117.90, 120.13, 121.10, 122.34, 123.77, 124.29, 131.67, 136.64.

Preparation of Bis(fluorosulfonyl)amide Ionic Liquids

1c. Synthesis of 1-butyl-3-methylimidazolium bis(fluorosulfonyl)amide (Bmim FSA)

1-butyl-3-methylimidazolium bromide (20.00 g, 0.09127 mol) dissolved in 30 mL deionized water was reacted with one equivalent of lithium bis(fluorosulfonyl)amide (20.01 g, 0.09127 mol) dissolved in 30 mL deionized water in a round bottom flask containing a stir bar. The reaction mixture was left to stir at room temperature for 24 hours. The resulting pale-yellow ionic liquid was washed with deionized water until the wash tested negative for residual bromide with 50 mM aqueous silver nitrate. The product was rotary evaporated and dried in a high vacuum oven at 60 ˚C for several days. The final product was a pale yellow, viscous liquid (25.04 g, 86 %, molar mass: 319.36 g/mol, water content: 25 ppm). ^{1}H (400 MHz; DMSO-d_6) δ 0.89-0.93 (t, 3H), 1.24-1.30 (m, 2H), 1.74-1.81 (m, 2H), 3.85 (s, 3H), 4.14-4.18 (t, 2H), 7.68 (s, 1H), 7.75 (s, 1H), 9.10 (s, 1H); ^{13}C (101 MHz; DMSO-d_6) δ 13.18, 18.72, 31.30, 35.67, 48.47, 122.20, 123.56, 136.44.

2c. Synthesis of 1-(2-methoxyethyl)-3-methylimidazolium bis(fluorosulfonyl)amide (EOMmim FSA)

1-(2-methoxyethyl)-3-methylimidazolium bromide (26.31 g, 0.1190 mol) dissolved in 20 mL deionized water was reacted with one equivalent of potassium bis(fluorosulfonyl)amide (26.09 g, 0.1190 mol) dissolved in 30 mL deionized water in a round bottom flask containing a stir bar. The reaction mixture was left to stir at room temperature for 24 hours. The resulting yellow ionic liquid was washed with cold deionized water until the wash tested negative for bromide with 50 mM aqueous silver nitrate. The product was rotary evaporated and dried in a high vacuum oven at 60 °C for several days. The final product was a yellow, viscous liquid (19.24 g, 49 %, molar mass: 321.32 g/mol, water content: 70 ppm). ^{1}H (400 MHz; DMSO-d_6) δ 3.27 (s, 3H), 3.67-3.69 (t, 2H), 3.86 (s, 3H), 4.33-4.36 (t, 2H), 7.67-7.68 (t, 1H), 7.70-7.71(t, 1H), 9.07 (s, 1H), ^{13}C (101 MHz; DMSO-d_6) δ 35.73, 48.66, 58.04, 69.57, 122.61, 123.44, 136.80.

3c. Synthesis of 1-allyl-3-methylimidazolium bis(fluorosulfonyl)amide (Amim FSA)
1-allyl-3-methylimidazolium chloride (25 g, 0.1576 mol) dissolved in 30 mL deionized water was reacted with one equivalent of potassium bis(fluorosulfonyl)imide (34.55 g, 0.1576 mol) dissolved in 40 mL deionized water in a round bottom flask containing a stir bar. The reaction mixture was left to stir at room temperature for 24 hours. The resulting ionic liquid was washed with deionized water until the wash tested negative for chloride using 50 mM aqueous silver nitrate. The product was rotary evaporated and dried in a high vacuum oven at 70 ˚C for 48 hours. The final product was a very pale yellow, viscous liquid (40.20 g, 84%, molar mass: 303.30 g/mol, water content: 9 ppm). ^{1}H (400 MHz; DMSO-d_6) δ 3.86 (t, 3H), 4.82-4.83 (d, 2H), 5.28-5.38 (m, 2H), 6.00-6.08 (m, 1H), 7.67 (d, 2H), 9.08 (s, 1H), 13C (101 MHz; DMSO-d_6) δ 35.79, 50.86, 120.25, 122.33, 123.77, 131.60, 136.64.

Preparation of Ionic Liquid-Single-Walled Carbon Nanotube Mixtures

All mixtures were prepared in a low-moisture dry box under compressed air. Based on the density of each IL, mixtures were prepared with three mL of ionic liquid and 0.5, 2 or 5 wt% of SWCNTs. The mixtures were sonicated for 120-minute periods in sealed vials of the similar dimensions using a VWR Ultrasonic Cleaner Model 97043-992 water bath sonicator. The IL-SWCNT dispersions remained stable for several months. Sonication time of less than 120 minutes did not result in stable IL-SWCNT mixtures with improved conductivity values. A hand grinding method attempted using a mortar and pestle also did not result in consistently uniform IL-SWCNT combinations with improved conductivity values.

Characterization of Ionic Liquid-Single-Walled Carbon Nanotube Mixtures

Viscosities of pure ILs and IL-SWCNTs mixtures were measured with a Cambridge Applied Systems ViscoLab 4100 electromagnetic reciprocating piston viscometer that was temperature regulated by a Lauda RM-6 recirculating water bath.

Electrochemical Impedance Spectroscopy - Variable Temperature Ionic Conductivities:
IL-SWCNT samples were packed in a dry nitrogen atmosphere into an airtight 3 mL (Biologic Brand) two-electrode sample cell, leaving 50% of the cell volume available for thermal expansion. The cells were temperature controlled from 15 °C to 90 °C using a silicone oil bath. The electrochemical impedance measurements were done using a Solartron 1260 Impedance Analyzer coupled with a Solartron 1287 Electrochemical

Interface. Experimental parameters utilized a frequency sweep from 25 Hz to 2.5 MHz using a resolution of 20 data points per decade, and the energization was set with an AC amplitude of 10 mV with no DC offset. The resulting Nyquist plot of reactance versus resistance was inspected to determine the real electrical resistance. Using the corresponding cell constants and the electrical resistance, conductivity was calculated and plotted versus temperature. The data shown and discussed are the averages of three sets of measurements.

Results and Discussion

Electrochemical impedance spectroscopy of the ionic liquid-single walled carbon nanotube (IL-SWCNT) mixtures was performed over a wide temperature range (15 to 85 °C; 288 to 358 K) in order to obtain information about the nature of the conductivity (σ) of each composite. Conductivity values were obtained from corresponding Nyquist plots. As shown in Tables I and II, the conductivity of the IL-SWCNTs composites depended on temperature, cation and anion types, and SWCNT concentration.

Due to the composite nature of the mixtures, the resulting conductivity is due to the bulk IL, IL-solid interface, and SWCNT contributions. The SWCNTs are comprised of metallic and semiconducting nanotubes, and their electrical conductivity results from the motions of both electrons and holes. In the IL, the ionic conductivity is due to the motions of both the cations and anions. The IL transport properties depend on the structure of the IL, as determined by the composition of the ions and their intermolecular interactions. In imidazolium ILs, in addition to hydrogen bonding and Coulombic interactions, there are Van der Waals, polarization, π–π, and dipole−dipole interactions between the ions (44). In the imidazolium ILs studied here, the side chain functionality varied from alkyl to allyl to ether and the associated anions varied in size and dynamical complexity (from FSA^- to NTf_2^-).

TABLE I. Viscosities and Temperature-Dependent Conductivities of NTf_2 Ionic Liquids and NTf_2 Ionic Liquid-Single-Walled Carbon Nanotube Mixtures.

Cation and SWCNT content	Viscosity cP, 25 °C	Conductivity (σ, mS/cm), at temperature (°C)							
		15	25	35	45	55	65	75	85
Bmim	50	3.9	5.0	6.3	8.0	10.1	12.8	16.2	20.5
Bmim + 2 wt% SWCNTs	*	19.2	25.1	42.9	52.6	60.0	66.6	75.7	89.1
Bmim + 5 wt% SWCNTs	*	268	277	287	298	309	322	335	350
Amim	34	6.8	8.4	10.5	13.0	16.2	20.1	25.0	31.0
Amim + 0.5 wt% SWCNTs	-	8.3	11.0	15.7	20.4	26.0	32.0	34.4	37.9
Amim + 2 wt% SWCNTs	*	17.3	24.3	33.9	44.6	54.0	65.4	76.1	90.5
Amim + 5 wt% SWCNTs	*	475	496	490	511	506	529	525	530
EOMmim	45	3.3	4.7	6.5	8.9	11.8	15.0	18.4	21.7
EOMMIM + 2 wt% SWCNTs	*	8.8	14.6	17.3	27.4	35.7	48.1	57.1	72.6
EOMmim + 5 wt% SWCNTs	*	-	540	556	578	594	610	635	657

* Viscosity higher than 10,000 cP.

TABLE II. Viscosities and Temperature-Dependent Conductivities of FSA Ionic Liquids and FSA Ionic Liquid-Single-Walled Carbon Nanotube Mixtures.

Cation and SWCNT content	Viscosity cP, 25 °C	Conductivity (σ, mS/cm), at temperature (°C)							
		15	25	35	45	55	65	75	85
Bmim	33	7.9	9.7	11.9	14.7	18.1	22.4	27.6	34.0
Bmim + 2 wt% SWCNTs	*	39.7	47.4	57.4	70.9	84.8	101	116	132
Bmim + 5 wt% SWCNTs	*	87.1	76.7	78.1	83.7	88.8	91.7	98.1	102
Amim	25	12.5	15.1	18.3	22.1	26.7	32.3	39.0	47.2
Amim + 0.5 wt% SWCNTs	-	14.3	18.7	23.5	29.9	32.5	39.7	47.6	53.0
Amim + 2 wt% SWCNTs	*	63.7	77.2	93.4	112	126	134	146	168
Amim + 5 wt% SWCNTs	*	404	382	406	417	432	453	465	480
EOMmim	30	-	8.0	10.8	14.7	18.2	22.9	27.7	32.7
EOMMIM + 2 wt% SWCNTs	*	-	30.1	33.4	43.4	62.7	130	163	228
EOMmim + 5 wt% SWCNTs	*	-	176	189	194	208	208	234	262

* Viscosity higher than 10,000 cP.

For liquid systems, the ionic conductivity can be qualitatively described by the Nernst-Einstein (NE) equation [1]. Here the ionic conductivity (σ) depends mainly on temperature (T), the number of available charge carriers (c), and the self-diffusion coefficient (D). Connecting the ionic conductivity to the viscosity (η) is accomplished by the self-diffusion coefficient (D) through the Stokes-Einstein (SE) relationship [2], Here q, k_B, and r represent the charge of the carrier, Boltzmann constant, and hydrodynamic radius, respectively. It should be understood that both equations were developed for applications to very dilute solutions and that in these solutions, the ions are depicted as hard non-interacting spheres, moving through a continuum of viscosity η. The ions are also expected to be single entities.

$$\sigma = \frac{Dq^2c}{k_BT} \quad [1]$$

$$D = \frac{k_BT}{4\pi r\eta} \quad [2]$$

Since the IL-SWCNT mixtures are not dilute nor purely ionic, the NE and SE relationships will be used sparingly in the discussions that follow.

Temperature and Nanotube Concentration Effects

As shown in Tables I and II, an increase in SWCNT concentration significantly increased σ, with the largest enhancement (up to 540 mS/cm at 25 °C) being observed for the 5 wt% composites, regardless of temperature, and anion and cation types. Figure 2 is a graph of the temperature-dependent conductivity values obtained for a representative IL-SWCNT system - pure EOMmim NTf_2 and the corresponding 2 wt% and 5 wt% SWCNT composites. As shown, increased conductivity was observed as SWCNT concentration increased. From the NE equation, at a specific temperature an increase in charge carrier concentration will cause an increase in the conductivity. Conductivity increased with temperature in a similar fashion for the 0 and 2 wt% SWCNT samples,

while it rose only slightly for 5 wt% SWCNT. Similar trends were observed with the other pure ILs and their corresponding SWCNT composites.

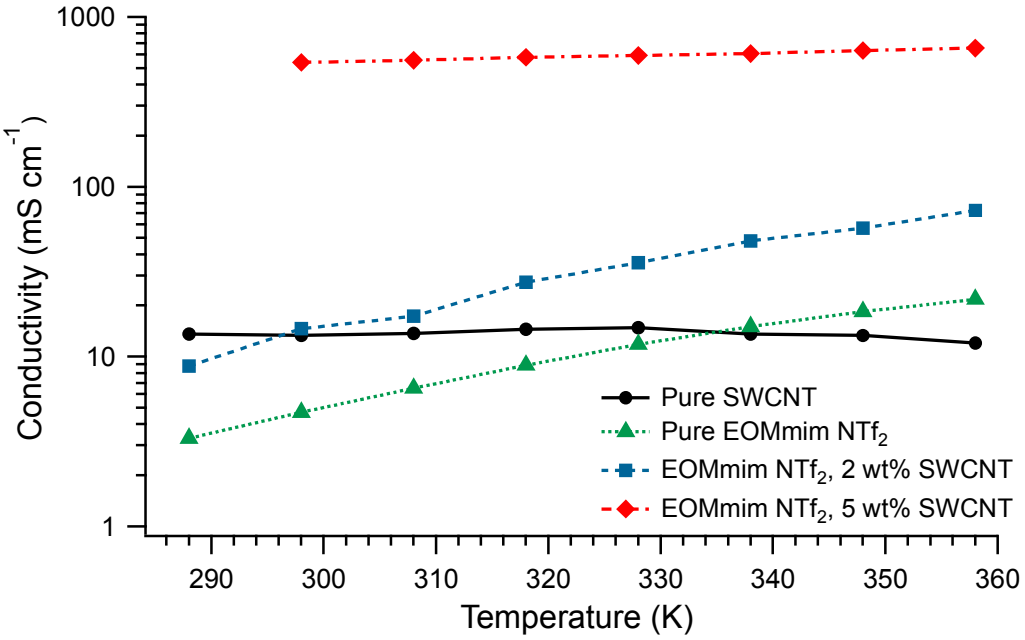

Figure 2. Temperature-dependent conductivities of pure EOMmim NTf_2 and its 2 and 5 wt% SWCNT mixtures, compared to pure SWCNT for reference, obtained from EIS Nyquist plots. Numerical values are given in Table I. Similar trends were observed with the other pure ILs and their corresponding mixtures.

From the NE and SE relationships, it is expected that an increase in conductivity results from a decrease in liquid solution viscosity. The viscosities of the pure ILs decrease with increasing temperature in a non-Arrhenius fashion typical of ILs. However, the addition of the SWCNTs significantly increased the viscosity of the composites to beyond the range of our instrumentation (>10,000 cP). Despite the dramatic increase in viscosity, the conductivities of the 0.5 and 2 wt% SWCNT mixtures are factors of 1.1-1.6 and 2.5-7 times larger than the conductivities of their respective pure ILs over the temperature ranges measured. In addition, the conductivities of the 0.5 and 2 wt% SWCNT mixtures have very similar, non-Arrhenius temperature dependences as those of their respective pure ILs. From this behavior we infer that the nanotubes contribute significantly to the conductivity of the mixtures in this concentration regime, but charge transport is still regulated by the dynamics of the ILs, which is linked to their viscosities.

In contrast, the conductivities for the 5 wt% SWCNT mixtures follow Arrhenius behavior with a much weaker temperature dependence than the lower-concentration mixtures and pure ILs. For comparison we include in Figure 2 our own measurements for pure SWCNTs, which were fairly constant over the entire temperature range. Generally, the temperature dependence of the electrical conductivity in semiconductors increases with increasing temperature. Although the measured values ranging from 12-14.8 mS/cm are very small compared to reported values (~ 10^2 to 10^6 S/cm) (14), it should be pointed out that in our measurements, the platinum probes of the BioLogic cell are immersed into

the SWCNTs. Therefore, proper contact between the electrodes and the SWCNTs was lacking. Generally, in conductivity measurements on CNTs, a CNT sheet or sputtered wires of CNTs onto a solid surface are used to ensure proper contact (45). Despite this, the data is useful in that it can be used as a representation of the temperature dependence of the conduction process in the nanotubes, which as shown in Figure 2, differs from that of the pure IL and even the 2 wt% mixture. However, it is quite similar to the 5 wt% EOMmim NTf_2/SWCNT mixture and those observed for the other IL-SWCNT mixtures as well, suggesting the conduction process of those mixtures is dominated by that of the SWCNTs.

To further illustrate the differences in conductivity mechanisms between lower and higher SWCNT loadings, we obtained activation energies for conductivity from Arrhenius fits of the variable-temperature conductivity data. Although some data sets clearly show curvature, linear Arrhenius fits were sufficient to indicate a clear difference between the behavior of all six IL-SWCNT combinations at 5 wt% loading versus lower loadings, as shown in Table III. The difference is that the activation energies are small for the 5% loadings (1.3 to 5.7 kJ/mol) while for the 0.5 and 2 wt% loadings the activation energies are large and generally comparable to those of the corresponding pure ILs (11.5 to 25.6 kJ/mol). This is clear evidence for a conductivity mechanism at the 5 wt% loading level that is based on the charge transport properties of the nanotubes, and that the role of the IL in this regime is to suspend the nanotubes in a manner that facilitates nanotube-centered transport and makes good contact with the conductivity probe electrodes.

TABLE III. Activation Energies for the Conductivity of Pure Ionic Liquids and Ionic Liquid-Single-Walled Carbon Nanotube Mixtures.

Cations	Activation Energy, kJ/mol	
	NTf_2 anion	**FSA anion**
Bmim	23.5 ± 0.4	20.6 ± 0.3
Bmim + 2 wt% SWCNTs	18.3 ± 1.8	15.1 ± 0.2
Bmim + 5 wt% SWCNTs	3.2 ± 0.1	4.4 ± 0.2
Amim	21.1 ± 0.3	18.4 ± 0.3
Amim + 0.5 wt% SWCNTs	19.3 ± 1.2	15.9 ± 0.5
Amim + 2 wt% SWCNTs	20.0 ± 0.8	11.5 ± 0.6
Amim + 5 wt% SWCNTs	1.3 ± 0.2	3.3 ± 0.1
EOMmim	23.5 ± 0.6	20.9 ± 0.4
EOMmim + 2 wt% SWCNTs	25.6 ± 0.9	19.1 ± 0.6
EOMmim + 5 wt% SWCNTs	2.7 ± 0.1	5.7 ± 0.4

As discussed above, at lower SWCNT loadings (0.5 and 2 wt%), conductivities increase over those of the pure IL despite very large increases in viscosity. Given the very high intrinsic conductivity of the nanotubes, it is reasonable to assume that they make a large contribution to the conductivity mechanism, but the temperature dependences indicate that IL dynamics still regulates charge transport. This could be due to the Brownian fluctuations of the IL ions inducing field fluctuations and polarized charges in the nanotubes that inhibit longitudinal charge transport within the nanotubes. The result of this polarizing effect would be a distribution of regimes with varying ion dynamics throughout the mixture, which can contribute incoherently to the conductivity. We

hypothesize that at the higher 5 wt% loading, fluctuations in the IL are reduced and it is behaving like a confined fluid where the dynamics are frozen out. We are looking at ways to test this hypothesis.

Cation and Anion Effects

As mentioned above, we selected three imidazolium cations and two sulfonylamide anions to investigate how changes in IL-nanotube interactions affect the conductivities of the composite systems. In fact, some clear patterns in the conductivity data are apparent, as shown in Figure 3. For SWCNT loadings up to 2 wt%, the conductivities of the composites track in opposite order with the viscosities of their constituent ILs, as they do in the pure ILs. Thus FSA^- anion-based IL composites have higher conductivities compared to the NTf_2^- analogues, because the viscosities of the FSA^- salts are lower and, as discussed above, IL dynamics play a role in charge transport in the regime up to 2 wt% SWCNT.

Between 2 and 5 wt% SWCNT the trend between the two anion families is reversed, with the NTf_2^- anion-based 5 wt% composites having greater conductivities compared to their FSA^- analogues (see Figure 3). In this regime, the activation energies indicate that IL dynamical properties such as viscosity are not a factor in the conductivity mechanism. Instead, we must look in the direction of structural differences in the IL-nanotube interactions, considering that the trifluoromethyl groups on the NTf_2^- anion may impose steric or packing factors on the interactions that are lacking in the FSA^- case, or that FSA may have a more polarizing effect on the nanotube, changing the energetic landscape of charge transport. In the future, these hypotheses can be tested by substituting other perfluoroalkylsulfonylamide anions or other types of anion families.

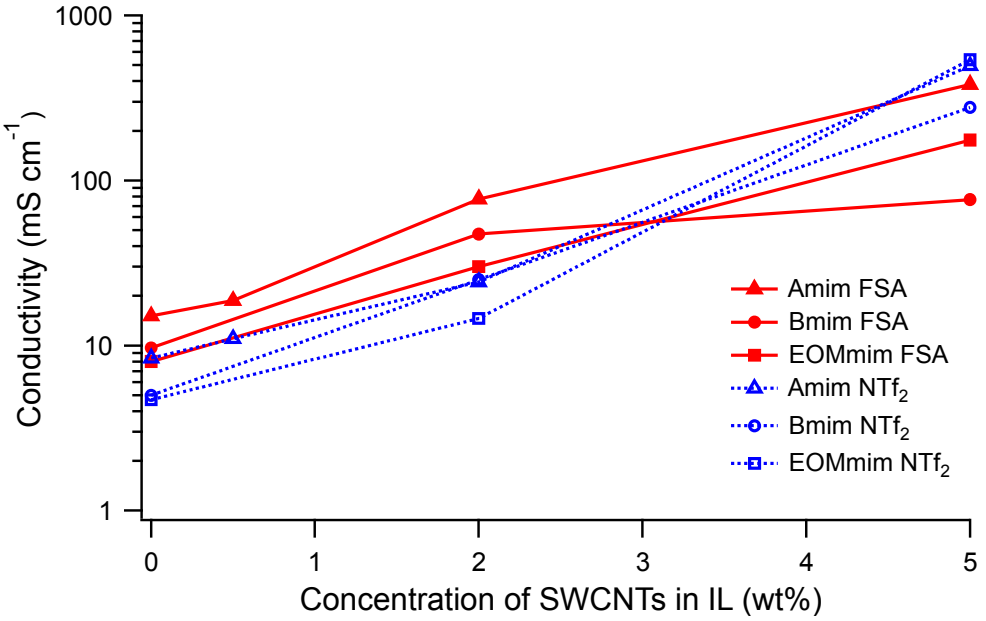

Figure 3. Conductivity of IL-SWCNT mixtures containing 0 - 5 wt% SWCNTs, at 25 °C.

Figure 3 also shows interesting patterns among the three chosen cations. At 2 wt% loading and below, the conductivity trends of the cations basically follow the viscosities of their respective ILs. However at 5 wt% loading, the $EOMmim^+$ and $Amim^+$ composites show higher conductivities than the $Bmim^+$ composites. The precise reasons for this may need to be elucidated by molecular dynamics calculations or interface-selective spectroscopy techniques. We have postulated that the allyl group of $Amim^+$ might provide additional interaction with the π-orbital system of the nanotube. In the case of $EOMmim^+$, the ether group alters anion-cation hydrogen bonding interactions, with impacts on the structure of the IL phase (39-43). The $Bmim^+$ cation appears to be least effective in promoting conductivity at 5 wt% loading. Although the butyl chain is too short to induce polar/non-polar domain segregation in the bulk IL, it may have a steric or structural organizational effect on the IL-nanotube interaction that makes it less favorable in promoting conductivity. This idea can be tested by substituting shorter- ($Emim^+$) or longer-chain ($Hmim^+$, $Omim^+$) cations, which we will do in subsequent studies.

Conclusion

The temperature-dependent conductivity profiles of six IL-SWCNT composites were studied over a wide range of nanotube concentrations. Between 0 and 2 wt% SWCNT loading, the presence of nanotubes increased the conductivity by factors up to 7-fold, despite the fact that the viscosities of the IL-SWCNT composites were very high. Within this concentration range, the temperature dependences of the conductivities indicated that IL dynamics still regulates the enhanced charge transport. The performance of the composites was generally inversely related to the relative viscosities of the pure IL components.

The mechanism of conductivity was clearly different at 5 wt% SWCNT loading for all six ILs. This loading is higher than generally reported in other literature, and it provided some provocative results. Remarkably, conductivity values of 540 mS cm^{-1}, 496 mS cm^{-1} and 382 mS cm^{-1} were obtained for 5 wt% SWCNT mixtures containing EOMmim NTf_2, Amim NTf_2, and Amim FSA, respectively. The activation energies for all six 5 wt% composites were much smaller than they were for the lower SWCNT loading regime, and comparable to the behavior of pure SWCNTs. It appears that the role of the IL in the 5 wt% regime is to suspend the nanotubes in a manner that facilitates nanotube-centered transport and makes good contact with the conductivity probe electrodes. Concurrent with the change in mechanism at 5 wt% loading, the ranking of conductivity as a function of anion flips, such that the composites with NTf_2^- anions have higher conductivities than their FSA^- congeners, the opposite of the lower loading regime where the lower viscosities of the FSA^- ILs benefit the conductivities of their composites. The reason for this inversion in ranking can be explored by substituting with other perfluoroalkylsulfonylamide anions (46) to elucidate the effects of anion structure on IL-SWCNT interactions.

Examining the effects of different functional groups on the IL cations provided interesting results. At low loadings, the effects of cation substitution on IL-SWCNT composite conductivity are traceable to their influence on the viscosities of the pure ILs. At 5 wt% loading, there is evidence that differential IL-SWCNT interactions depend on the identity of the functional group, in ways that could facilitate or possible inhibit charge

transport. Interestingly, the aliphatic imidazolium cation $Bmim^+$ performed worse than $EOMmim^+$ and $Amim^+$, which has interesting implications for prior work that has mainly been focused on 1-alkyl-3-methylimidazolium ILs. This finding suggests that further investigation with shorter- ($Emim^+$) or longer-chain ($Hmim^+$, $Omim^+$) cations, as well as other types of ether-substituted imidazolium cations (41), is warranted. Future work will involve spectroscopic (Mid-IR and Raman) analyses on the IL-SWCNT mixtures to better understand the interaction between the ILs and the SWCNTs. In addition, the efficiency of these unique electrode-electrolyte mixtures in supercapacitors will be determined.

Acknowledgments

The authors thank the National Institutes of Health (NIH), Research Initiative for Minority Students (RIMS) Program (NIH 5R25GM065096) at the City University of New York for student internship support. The synthesis of the mixtures was supported by the Professional Staff Congress-City University of New York Grants (# 69297-00 47 and 50) and the CUNY Advanced Science Research Center Faculty Fellows Program 2018. The IL physical characterization work at BNL was supported by the U.S. Department of Energy, Office of Basic Energy Sciences, Division of Chemical Sciences, Geosciences, and Biosciences under contract DE-SC0012704. The ionic conductivity measurements performed at Brooklyn College/CUNY was supported by the National Science Foundation, Solid State and Materials Chemistry Program, Division of Materials Research, EAGER award #1841398.

References

1. Poonam, K. Sharma, A. Arora and S. K. Tripathi, *J. Energy Storage*, **21**, 801 (2019).
2. M. Winter and R. J. Brodd, *Chem. Rev.*, **104**, 4245 (2004).
3. A. Dive and S. Banerjee, *J. Electrochem. Energy Convers. Storage*, **15**, 011001 (2017).
4. Q. Cheng, J. Tang, J. Ma, H. Zhang, N. Shinya and L.-C. Qin, *Phys. Chem. Chem. Phys.*, **13**, 17615 (2011).
5. A. Burke, *J. Power Sources*, **91**, 37 (2000).
6. M. F. El-Kady, V. Strong, S. Dubin and R. B. Kaner, *Science*, **335**, 1326 (2012).
7. Y. Zhu, S. Murali, M. D. Stoller, K. J. Ganesh, W. Cai, P. J. Ferreira, A. Pirkle, R. M. Wallace, K. A. Cychosz, M. Thommes, D. Su, E. A. Stach and R. S. Ruoff, *Science*, **332**, 1537 (2011).
8. H. J. In, S. Kumar, Y. Shao-Horn and G. Barbastathis, *Appl. Phys. Lett.*, **88**, 083104 (2006).
9. P. Simon and Y. Gogotsi, *Nat. Mater.*, **7**, 845 (2008).
10. C. Liu and H.-M. Cheng, *J. Phys. D, Appl. Phys.*, **38**, R231 (2005).
11. J. N. Coleman, U. Khan, W. J. Blau and Y. K. Gun'ko, *Carbon*, **44**, 1624 (2006).
12. A. Chou, T. Böcking, R. Liu, N. K. Singh, G. Moran and J. J. Gooding, *J. Phys. Chem. C*, **112**, 14131 (2008).
13. M. Burghard, *Surf. Sci. Rep.*, **58**, 1 (2005).

14. Q. Cao, Q. Yu, D. W. Connell and G. Yu, *Clean Technol. Environ. Policy*, **15**, 871 (2013).
15. R. H. Baughman, A. A. Zakhidov and W. A. de Heer, *Science*, **297**, 787 (2002).
16. R. Saito, M. Fujita, G. Dresselhaus and M. S. Dresselhaus, *Appl. Phys. Lett.*, **60**, 2204 (1992).
17. K. H. An, W. S. Kim, Y. S. Park, J.-M. Moon, D. J. Bae, S. C. Lim, Y. S. Lee and Y. H. Lee, *Adv. Funct. Mater.*, **11**, 387 (2001).
18. A. Izadi-Najafabadi, S. Yasuda, K. Kobashi, T. Yamada, D. N. Futaba, H. Hatori, M. Yumura, S. Iijima and K. Hata, *Adv. Mater.*, **22**, E235 (2010).
19. W. S. Zhang, W. J. Xu, F. Zhang, Y. Z. Wang, J. Li, B. A. Wang and Y. Li, *J. Chin. Chem. Soc.*, **59**, 753 (2012).
20. S. Kazemiabnavi, Z. Zhang, K. Thornton and S. Banerjee, *J. Phys. Chem. B*, **120**, 5691 (2016).
21. S. Lall-Ramnarine, S. Suarez, N. Zmich, D. Ewko, S. Ramati, D. Cuffari, M. Sahin, Y. Adam, E. Rosario, D. Paterno and J. Wishart, *ECS Trans.*, **64**, 57 (2014).
22. G. A. Snook, P. Kao and A. S. Best, *J. Power Sources*, **196**, 1 (2011).
23. T. Fukushima, K. Asaka, A. Kosaka and T. Aida, *Angew. Chem. Int. Edit.*, **44**, 2410 (2005).
24. T. Fukushima, A. Kosaka, Y. Ishimura, T. Yamamoto, T. Takigawa, N. Ishii and T. Aida, *Science*, **300**, 2072 (2003).
25. R. Hayes, G. G. Warr and R. Atkin, *Chem. Rev.*, **115**, 6357 (2015).
26. J. L. Bañuelos, G. Feng, P. F. Fulvio, S. Li, G. Rother, S. Dai, P. T. Cummings and D. J. Wesolowski, *Chem. Mat.*, **26**, 1144 (2014).
27. J. N. Israelachvili, *Intermolecular and Surface Forces*, Academic Press: New York, (2011).
28. R. Hayes, G. G. Warr and R. Atkin, *Phys. Chem. Chem. Phys.*, **12**, 1709 (2010).
29. W. Shi and D. C. Sorescu, *J. Phys. Chem. B*, **114**, 15029 (2010).
30. Y. Shim and H. J. Kim, *ACS Nano*, **3**, 1693 (2009).
31. K. Shimizu, C. E. S. Bernardes and J. N. Canongia Lopes, *J. Phys. Chem. B*, **118**, 567 (2014).
32. A. A. Freitas, K. Shimizu and J. N. Canongia Lopes, *J. Chem. Eng. Data*, **59**, 3120 (2014).
33. J. Wang, H. Chu and Y. Li, *ACS Nano*, **2**, 2540 (2008).
34. N. Hameed, J. S. Church, N. V. Salim, T. L. Hanley, A. Amini and B. L. Fox, *RSC Adv.*, **3**, 20034 (2013).
35. C. Kong, W. Qian, C. Zheng, Y. Yu, C. Cui and F. Wei, *Chem. Commun.*, **49**, 10727 (2013).
36. S. Lall-Ramnarine, C. Rodriguez, R. Fernandez, N. Zmich, E. Fernandez, S. Dhiman and J. F. Wishart, *ECS Trans.*, **75**, 215 (2016).
37. H. Tokuda, K. Hayamizu, K. Ishii, M. A. B. H. Susan and M. Watanabe, *J. Phys. Chem. B*, **109**, 6103 (2005).
38. S. J. Zhang, N. Sun, X. Z. He, X. M. Lu and X. P. Zhang, *J. Phys. Chem. Ref. Data*, **35**, 1475 (2006).
39. K. Shimizu, C. E. S. Bernardes, A. Triolo and J. N. Canongia Lopes, *Phys. Chem. Chem. Phys.*, **15**, 16256 (2013).
40. A. Triolo, O. Russina, R. Caminiti, H. Shirota, H. Y. Lee, C. S. Santos, N. S. Murthy and E. W. Castner, *Chem. Commun.*, **48**, 4959 (2012).

41. S. I. Lall-Ramnarine, M. Zhao, C. Rodriguez, R. Fernandez, N. Zmich, E. D. Fernandez, S. B. Dhiman, E. W. Castner and J. F. Wishart, *J. Electrochem. Soc.*, **164**, H5247 (2017).
42. G. D. Smith, O. Borodin, L. Y. Li, H. Kim, Q. Liu, J. E. Bara, D. L. Gin and R. Nobel, *Phys. Chem. Chem. Phys.*, **10**, 6301 (2008).
43. H. J. Zeng, M. A. Johnson, J. D. Ramdihal, R. A. Sumner, C. Rodriguez, S. I. Lall-Ramnarine and J. F. Wishart, *J. Phys. Chem. A*, **123**, 8370 (2019).
44. S. Zhang, J. Zhang, Y. Zhang and Y. Deng, *Chem. Rev.*, **117**, 6755 (2017).
45. B. Earp, D. Dunn, J. Phillips, R. Agrawal, T. Ansell, P. Aceves, I. De Rosa, W. Xin and C. Luhrs, *Mater. Res. Bull.*, **131**, 110969 (2020).
46. M. Zhao, B. N. Wu, S. I. Lall-Ramnarine, J. D. Ramdihal, K. A. Papacostas, E. D. Fernandez, R. A. Sumner, C. J. Margulis, J. F. Wishart and E. W. Castner, *J. Chem. Phys.*, **151**, 074504 (2019).